Available online at www.sciencedirect.com
SCIENCE DIRECT®
ELSEVIER
International Journal of Multiphase Flow 30 (2004) 431–454
International Journal of Multiphase Flow
www.elsevier.com/locate/ijmulflow

A 2-D model of Rayleigh instability in capillary tubes—surfactant effects

D. Campana [a,b], J. Di Paolo [b], F.A. Saita [a,*]

[a] *Instituto de Desarrollo Tecnológico para la Industria Química (INTEC), UNL, CONICET, Santa Fe, Argentina*

[b] *Facultad De Ingeniería, UNER, Oro Verde, Entre Ríos, Argentina*

Received 9 February 2003; received in revised form 21 March 2004

Abstract

The Rayleigh instability of stagnant liquid films lining the interior of capillary tubes is analyzed with the aid of a 2-D free surface flow model; this axisymmetric model is previously validated using already published theoretical and experimental results. The Galerkin-finite element method is used to transform the complete set of governing equations and boundary conditions into a discrete set, which is then simultaneously solved at each time step by Newton's method. Predictions of well known simplified models represented by nonlinear evolution equations derived on the one-dimensional flow assumption are compared with those obtained from the present one. The comparisons are made for pure liquids and also for liquids contaminated with insoluble surfactants; they show that the simpler models represent the free surface evolution reasonable well. However, the 1-D models generally underestimate the time needed to complete the unstable process that ends—if the film is thick enough—when the inner gas phase becomes disconnected due to the formation of liquid lenses regularly spaced; these discrepancies become larger when surface active agents are present. Surfactant effects and the wealth of information produced by the 2-D model are both evidenced through sample results presented at the end of the paper.

Keywords: Rayleigh instability; Insoluble surfactants; Numerical analysis

* Corresponding author.
E-mail address: fasaita@ceride.gov.ar (F.A. Saita).

0301-9322/$ - see front matter © 2004 Elsevier Ltd. All rights reserved.
doi:10.1016/j.ijmultiphaseflow.2004.03.007

1. Introduction

Thin liquid films lining the inner surface of a capillary tube, or coating the external surface of a filament, are known to be unstable to axially symmetric surface perturbations whose wavelengths are of the order of (or larger than) $2\pi r_0$, where r_0 is the location of the unperturbed gas–liquid interface measured from the axis of symmetry.

Lord Rayleigh, near the end of the 19th century, was the first to analyze this type of instability; then, except for a few works among which the studies of Weber (1931) and Tomotika (1935) are significant, the subject did not call the attention of the scientific world until 1962 when the linear stability analysis of Goren was published. For axially symmetric perturbations, Goren determined the most unstable modes when either inertia or viscous forces are negligible. At that time it became evident that annular thin films have important implications in biological processes as well as in industrial ones, this fact motivated the interest for studying the phenomena that lead to their formation and breakup.

Annular liquid films are formed when long bubbles or drops displace a liquid contained in a capillary tube. The moving front of the invading phase leaves behind a uniform thin film of the displaced liquid surrounding the intruding phase. However, the film is unstable to certain perturbations and evolves to form almost regularly spaced unduloids or, if the thickness of the film is large enough, the unduloids grow until the tube inner gap is bridged by liquid lenses and the invading phase becomes discontinuous. The time elapsed between the former steps of the instability and the formation of the liquid bridge is named as 'closure time'.

The phenomena just described have close connections with diverse real situations like the intrusion of air displacing water from a mat of fibers in papermaking processes, or the formation of lenses in the small airway of the lung when a disease known as respiratory stress syndrome, commonly present in premature neonates, occurs. Also, they might be regarded as a simplified model of the events occurring at pore level when oil bearing strata are invaded by water, as it happens in secondary oil recovery processes.

On the other hand, for a film deposited on the external wall of a capillary tube or onto a filament, a similar instability process will end up forming an almost regular pattern of equally spaced droplets. This phenomenon which is frequently observed on threads, or on spider's web, as a consequence of atmospheric moisture condensed at nights, also occurs when wires or optical fibers are coated for isolating or protecting purposes (Queré, 1999).

In order to explain the underlying mechanism governing the behaviors described above, several experimental and theoretical studies have been carried out since the work of Goren was published. Significant experimental data were given by Goldsmith and Mason (1963) and by Gauglitz and Radke (1988). Theoretical models were also developed; however, they were almost exclusively directed to elucidate working principles and malfunctions of the pulmonary system, in particular about regions of the lung where the flow of gases might be arrested restraining the primary function of this organ; i.e. to allow the oxygen and carbon dioxide to be interchanged between air and blood. Considering the geometry of these regions, which are characterized by small airway conduits lined by thin liquid films, the mathematical representation of the problem was reduced to one-dimensional nonlinear evolution equations with the aid of lubrication theory.

These simple models were used at the beginning to determine the minimum amount of liquid (i.e. the critical film thickness) needed to produce the airway closure (Hammond, 1983; Gauglitz

and Radke, 1988). Afterwards, new features of the problem were introduced with subsequent model refinements; Johnson et al. (1991) roughly considered the effect of inertia and determined the timescales characterizing the formation of unduloids and liquid bridges. Halpern and Grotberg (1992) examined the effects of airway flexibility; the introduction of wall compliance resulted in a dramatic change in the values of the critical film thickness. Finally, Otis et al. (1993) and Halpern and Grotberg (1993) took in account the presence of insoluble surfactants adsorbed at the interface; the conclusion they arrived at is that surfactants do not alter the critical film thickness, but they delay the instability process and the time needed to produce the airway closure might be four to five times longer than in the case of a clean interface. More recently, by means of linear stability analysis Kwak and Pozrikidis (2001) showed that the presence of insoluble surfactants reduces the growth rate of interfacial disturbances; also, they performed studies on nonlinear stability using lubrication approximation for rather thin films and found that surfactants do not affect the successive shapes adopted by the interface during the instability process; however, the growth rate of the interfacial waves is considerably delayed.

Despite their relative simplicity, the accuracy of these simplified models appear to be good enough for lung functioning examination; they produce reasonable estimations not only about airway closure times but also about the evolution of the free surface shapes along the process. Nonetheless, as we will see in the following sections, the predictions become less accurate with increasing initial film thickness or under the presence of surfactants; thus, in these cases a more realistic 2-D model should be employed. In addition, the simple models might be less successful in analyzing the instability process of a film deposited on a filament; this is so because in many cases of practical interest the thickness of the exterior film is—unlike the case of an inner film—as large as, or even larger than, the filament radius. In such an event the 1-D model might introduce large errors in the estimation of the time needed for the film to break down and to form equally spaced drops. This rupture time is a key feature to be known when the coated film has to be rapidly immobilized (e.g. by drying) before the instability develops undesirable thickness variations.

The 2-D free surface flow model employed in this work is rather general, with minor changes it can be adapted to study transient or steady state cases. Actually, it has been applied in the analysis of the steady displacement of pure liquids initially contained in small channels, by moving gas phases (Giavedoni and Saita, 1997, 1999); in that problem the presence of soluble surfactants has been considered too (Severino et al., 2003a,b). In the present work, as in several preceding papers (cf. Otis et al., 1993; Halpern and Grotberg, 1993; Kwak and Pozrikidis, 2001) only insoluble surfactants will be considered; nonetheless, even for soluble surfactants this approach can be acceptable since the phenomenon under analysis usually occurs in periods of time short enough that mass transfer between the bulk and the interface might be of little influence.

We here present the predictions obtained for stagnant films lining the inner walls of a capillary tube; this case was selected not only because the existence of analytical and experimental results that can be employed in the validation of our model, but also because we wish to determine the range of validity of the predictions obtained with the aid of the thin film approximation, in particular for cases where surfactants are present. We also wish to establish the curves of closure times versus Reynolds number for different values of relative initial film thickness when gravity forces are negligible (small capillaries).

In Section 2 we summarize the dimensionless governing equations of the model and the numerical technique employed; in Section 3 our model is validated by comparing the predictions

obtained with the theoretical results of Goren (1962) and also with experimental results produced by Goldsmith and Mason (1963). Computed predictions are presented in Section 4 which is divided into two subsections; in Section 4.1 we compare our results of airway closure times with those obtained from models represented by nonlinear evolution equations; the comparisons are made considering both pure liquids and liquids contaminated with insoluble surfactants. In Section 4.2 we first present our predicted dimensionless closure times when pure and contaminated liquids films of various initial thickness are lining the inner walls of capillaries. Then, we illustrate how the surfactants adsorbed at the interface change the values of the interfacial variables, and how this effects are transmitted to the bulk and the whole flow field is changed. Finally, Section 5 is devoted to conclusions.

2. Governing equations and numerical technique

2.1. Governing equations

Fig. 1 shows an inviscid gas phase surrounded by a stagnant liquid film deposited on the internal wall of a capillary tube of radius a; the gas–liquid interface is located at a distance b from the tube axis, thus, the relative thickness F of the initially uniform film is $(a-b)/a$. The incompressible liquid, which is assumed to be Newtonian of constant viscosity μ, density ρ and surface tension σ_c, is perturbed by a sinusoidal wave of amplitude ε_0 and wave-number α, and the film movement is studied. Since the analysis is performed on half wavelength, the domain extends π/α in the axial direction. The free surface location is parameterized in terms of the local film thickness h, and w and u are the velocity components in the axial and radial directions (z, r), respectively.

The governing equations of the flow problem are the mass balance and momentum balance equations, which in dimensionless form read as follows

$$\nabla \cdot \mathbf{v} = 0 \tag{1}$$

$$Re\left(\frac{\partial \mathbf{v}}{\partial t} + (\mathbf{v} - \dot{\mathbf{x}}) \cdot \nabla \mathbf{v}\right) = \nabla \cdot \mathbf{T} \tag{2}$$

where $\mathbf{T} = -p/Ca\mathbf{I} + (\nabla \mathbf{v} + \nabla \mathbf{v}^{\mathrm{T}})$.

In the foregoing the distances are measured in terms of the capillary radius (a), the units of measure for both velocity $\mathbf{v}$ and pressure p are given by $(\sigma_c F^3/\mu)$ and (σ_c/a) respectively, while the

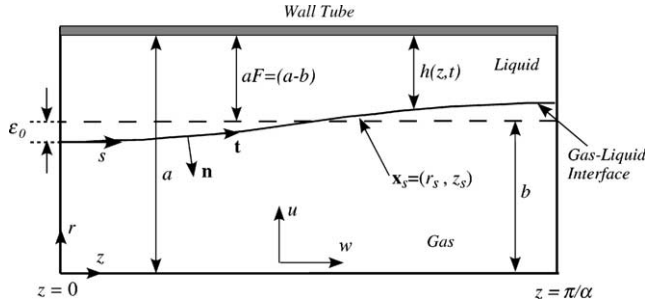

Fig. 1. Schematic representation of the problem, system of coordinates and basic dimensions.

components of the stress tensor $\mathbf{T}$ are measured in terms of $(\sigma_c F^3/a)$; accordingly the unit of time t results $(a\mu/\sigma_c F^3)$. Since the flow domain deforms due to the interfacial motion, we use an arbitrary Eulerian–Lagrangian (ALE) formulation; thus, in Eq. (2) the term $\dot{\mathbf{x}}$ accounts for the velocities of the domain coordinates. The coordinates are conveniently moved following the free surface expansion or contraction; for that purpose the term $\dot{\mathbf{x}}$ in Eq. (2) represents the velocities of the nodes in their vertical displacements, i.e. the nodes do not move in the axial direction. The nodes located at the interface follow the interfacial motion; that is, they always stay at the interface and their velocity is the interfacial velocity in the radial direction. The remaining nodes also move in the radial direction with a velocity that is proportional to the velocity of the corresponding interfacial node (i.e. at the same axial location); and the proportionality is given by the distance between the node and the capillary wall measured in terms of the local film thickness (see Giavedoni, 1995). In this way the whole domain stretches and shrinks following the motion of the interface.

The two dimensionless parameters appearing above are the modified Reynolds number $Re = (\rho a \sigma_c F^3)/\mu^2$, relating inertia, viscous and surface tension forces, and the Capillary number which in this case is $Ca = F^3$, giving the ratio between viscous and capillary forces.

The nonlinear system of equations just presented needs of initial and boundary conditions to be solved; as initial condition we impose an interfacial perturbation of the type

$$h(z,0) = F[1 + \varepsilon_0 \cos(\alpha z)] \tag{3}$$

where $\alpha = 2\pi a/\lambda$ is the wave-number of the perturbation. Since the wave pattern is repeated along the z-axis, our computational domain covers half wavelength only, and at both extremes ($z = 0$ and π/α) the following symmetry condition are imposed

$$w = 0; \qquad \frac{\partial u}{\partial z} = 0; \qquad \frac{\partial h}{\partial z} = 0 \tag{4}$$

The boundary conditions on the tube wall are the usual no-slip conditions ($u = w = 0$); in addition, it is assumed that no mass is transferred across the gas–liquid free surface, this boundary condition implies that the interface is a material surface and is mathematically represented by the kinematic equation:

$$(\mathbf{n} \cdot \mathbf{v})|_s = \mathbf{n} \cdot \dot{\mathbf{x}}_s \tag{5}$$

where the subscript (s) indicates that the terms are evaluated at the free surface.

Finally, we need to express the stress balance at the interface. In this work we assume that the gas phase is inviscid and of null pressure; therefore, the normal stresses in the liquid at the interface are equilibrated by the action of the local interfacial values of both surface tension and curvature, while the tangential stresses are equilibrated by the stresses originated in the gradients of the interfacial concentration of surfactant. This assumption implicitly disregard the interfacial viscous effects that surfactants might introduce. Therefore, in dimensionless form the stress balance equation at the interface is expressed as

$$\mathbf{n} \cdot \mathbf{T} = \frac{1}{Ca}[\sigma(2H)\mathbf{n} + \nabla_s \sigma] \tag{6}$$

where H represents the mean curvature, ∇_s is the interfacial gradient and σ is the local surface tension that depends upon the local concentration of solute (cf. Eq. (8)). The interfacial coordinates employed are the arc length (s) whose positive direction coincides with $\mathbf{t}$, the tangential unit

vector to the interface, and the azimuthal cylindrical coordinate (θ), which is normal to the plane defined by both axial and radial coordinates (see Fig. 1).

Since the surface tension depends upon the local concentration of surfactant, we should employ an expression for this functional relationship which, in general, is nonlinear. However, we will assume small departures from the uniform unperturbed initial conditions, only; therefore, a linear version of that expression is

$$\sigma^* = \sigma_m^* - \left(\frac{\partial \sigma^*}{\partial \rho^{s^*}}\right)\Bigg|_{\rho_m^{s^*}} (\rho^{s^*} - \rho_m^{s^*}) \tag{7}$$

where asterisks indicate dimensional quantities and the superscript (s) that they are evaluated at the interface.

In the preceding equation σ_m^* is the uniform surface tension that initially exist on the unperturbed interface and $\rho_m^{s^*}$ is the corresponding initial uniform concentration of adsorbed surfactant. Those are the quantities we choose as unit of measure for the dimensionless surface tension and interfacial concentration, respectively; thus, $\rho^s = \rho^{s^*}/\rho_m^{s^*}$ and $\sigma = \sigma^*/\sigma_m^*$, with $\sigma_c = \sigma_m^*$. Accordingly, the dimensionless version of Eq. (7) is

$$\sigma = 1 - \beta(\rho^s - 1) \tag{8}$$

where

$$\beta = \frac{\rho_m^{s^*}}{\sigma_m^*}\left(\frac{\partial \sigma^*}{\partial \rho^{s^*}}\right)\Bigg|_{\rho_m^{s^*}} \tag{9}$$

is a new dimensionless parameter that indicates how sensitive the surface tension is to variations of interfacial concentration of surfactant; actually, β is the slope of the curve $\sigma = f(\rho^s)$ at $\rho^s = 1$ and is known as elasticity number.

Considering Eq. (8), the stress balance equation at the interface can be rewritten as

$$\mathbf{T}\cdot\mathbf{n} = \frac{1}{Ca}[\sigma(2H)\mathbf{n} - \beta\nabla_s\rho^s] \tag{10}$$

Finally, the system of governing equations is completed with the following interfacial mass balance for the adsorbed solute:

$$\left(\frac{\partial \rho^s}{\partial t}\right)\Bigg|_{\mathbf{x}_{FS}} - \dot{\mathbf{x}}_s\cdot\nabla_s\rho^s + \rho^s v_{(\mathbf{n})}(\nabla_s\cdot\mathbf{n}) + \nabla_s\cdot(\rho^s\mathbf{v}^s) - \frac{1}{Pe_s}\nabla_s^2\rho^s = 0 \tag{11}$$

where $Pe_s = a\sigma_c F^3/(D_s\mu)$ is the interfacial Péclet number and D_s is the coefficient of interfacial diffusion of the adsorbed solute. In Eq. (11) $(\partial\rho^s/\partial t)|_{\mathbf{x}_{FS}}$ is the time variation of the interfacial concentration of solute measured at fixed surface coordinates ($\mathbf{x}_{FS}$), while $\dot{\mathbf{x}}_s$ represents the velocity of these coordinates with respect to the fixed reference frame shown in Fig. 1. $v_{(\mathbf{n})} = \mathbf{v}\cdot\mathbf{n}$ is the normal velocity component and $\mathbf{v}^s = (\mathbf{v}\cdot\mathbf{t})\mathbf{t}$ is the tangential velocity at the interface, respectively. Since we consider axisymmetric conditions, the interfacial gradient operator (∇_s) is simply: $((\mathrm{d}(\cdot)/\mathrm{d}s)\mathbf{t})$. This equation is solved imposing symmetry conditions at both ends of the domain ($z = 0$ and $z = \pi/\alpha$), i.e. the diffusive flux should be zero at these points.

Eq. (11) has been obtained under the following hypotheses:

(i) The interfacial diffusive flux can be represented by Ficks' law

$$\mathbf{j}^{s^*} = -D_s \nabla_s^* \rho^{s^*}$$

(ii) The interfacial diffusivity is isotropic and uniform.
(iii) The surfactant is insoluble, therefore the adsorption/desorption flux is null; for more details about Eq. (11) the reader might refer to Edwards et al. (1991) and Wong et al. (1996).

2.2. Numerical technique

The strongly coupled and highly nonlinear system of differential equations was transformed into an algebraic nonlinear set by employing the Galerkin-finite element technique; also, a suitable parameterization of the free surface was used. A key advantage in the application of the Galerkin-finite element method to free surface flows is the easiness by which the stress balance condition at the free surface (Eq. (10)) is imposed (Giavedoni, 1995; Giavedoni and Saita, 1997). In a very similar manner with the work of Giavedoni (1995), the flow domain is partitioned into a set of quadrilateral elements; each element is limited by two straight sides, formed by fixed spines of constant z coordinates, and by two curved sides which reflect the shapes of the free surface. This elements are mapped isoparametrically onto the unit square with coordinates (ξ, η), $0 \leqslant \xi, \eta \leqslant 1$, by means of the nine biquadratic basis functions ϕ^j used in the expansions representing the components of the velocity (see Eq. (14)),

$$\begin{aligned} z(\xi,\eta) &= \sum_{j=1}^{9} z^j \phi^j(\xi,\eta) \\ r(\xi,\eta,t) &= \sum_{j=1}^{9} r^j(t) \phi^j(\xi,\eta) \end{aligned} \tag{12}$$

where $(z^j, r^j(t))$ are the coordinates of the nodes. The free surface was parameterized using the just mentioned spines, a well known technique put forward by Kistler and Scriven (1983) by which the unknown parameters or variables representing the free surface location ($h^j(t)$) are conveniently handled so that the global system of equations, including those governing the shape and location of the free surface, can be simultaneously solved. Since the mesh adopted in this work has spines parallel to the r-axis, the coordinates of each node has a fixed value of z, a fact taken into account when building the Jacobian matrix in the numerical code. For the elements pertaining to the interface, the free surface in the computational domain is a line of constant η ($\eta = 1$), and it is approximated by the one-dimensional specialization of the biquadratic basis functions ($\tilde{\phi}^j = \phi^j(\xi, \eta = 1)$),

$$r_{\mathrm{FS}}(\xi,t) = 1 - \sum_{j=1}^{3} h^j(t) \tilde{\phi}^j(\xi) \tag{13}$$

In Eq. (13), the $h^j(t)$ are the coefficients of the gas–liquid interface parameterization; they represent the distance along a given spine from the wall to the free surface and are the unknowns that will be solved simultaneously with the system of equations.

Mixed interpolation was employed, i.e. biquadratic basis functions of nine nodes were used to interpolate velocities and coordinates, while bilinear ones of four nodes were employed for pressures, thus

$$\begin{aligned} \mathbf{v}(\mathbf{x},t) &= \sum_{j=1}^{9} \mathbf{v}^j(t)\phi^j(\xi,\eta) \\ p(\mathbf{x},t) &= \sum_{i=1}^{4} p^i(t)\psi^i(\xi,\eta) \end{aligned} \tag{14}$$

where $\mathbf{v}^j(t)$ and $p^i(t)$ are unknown time dependent nodal values and $\psi^i(\xi,\eta)$ are the four bilinear basis functions defined over the standard square.

Since the method summarized above is well known, the reader might refer to Giavedoni (1995) and Giavedoni and Saita (1997) for further details about the derivation of the residuals of weighted equations (momentum, mass and kinematic condition) and calculation of time derivatives. In what follows, we will concentrate on the interfacial mass balance of surfactant (Eq. (11)) and the way it is handled in the numerical scheme.

The weak form of the Galerkin weighted residual of the interfacial mass balance is obtained when Eq. (11), multiplied by a suitable trial function, is integrated on the interfacial area A:

$$\int_A \tilde{\phi}^k \left[\rho_t^s - \dot{\mathbf{x}}_s \cdot \nabla_s \rho^s + \rho^s v_{(\mathbf{n})} (\nabla_s \cdot \mathbf{n}) + \nabla_s \cdot (\rho^s \mathbf{v}^s) - \frac{1}{Pe_s} \nabla_s^2 \rho^s \right] \mathrm{d}A = 0, \quad k = 1, \ldots, n_{\mathrm{FS}} \tag{15}$$

where the index k runs through all interfacial nodes (n_{FS}) and the interfacial concentration is approximated by

$$\rho^s(t) = \sum_{m=1}^{3} \rho^{s^m}(t)\tilde{\phi}^m \tag{16}$$

In Eq. (15), ρ_t^s represents the first term of Eq. (11) and is the time derivative of the interfacial concentration at fixed free surface coordinates, while in Eq. (16) $\tilde{\phi}^m$ stands for the one-dimensional specialization of the biquadratic trial function employed in the expansions of velocities and coordinates as well; i.e. is the function already used to interpolate the free surface location (see Eq. (13)).

Eq. (15) can also be written as

$$\begin{aligned} &\int_A \left\{ \tilde{\phi}^k [\rho_t^s - \dot{\mathbf{x}}_s \cdot \nabla_s \rho^s] + \tilde{\phi}^k \rho^s v_{(\mathbf{n})} (\nabla_s \cdot \mathbf{n}) - \nabla_s \tilde{\phi}^k \cdot \rho^s \mathbf{v}^s + \frac{1}{Pe_s} (\nabla_s \tilde{\phi}^k \cdot \nabla_s \rho^s) \right\} \mathrm{d}A \\ &\quad + \int_A \nabla_s \cdot \left[\tilde{\phi}^k \rho^s \mathbf{v}^s - \frac{1}{Pe_s} \tilde{\phi}^k \nabla_s \rho^s \right] \mathrm{d}A = 0 \end{aligned} \tag{17}$$

then, if the differential area is expressed as $r_s \, \mathrm{d}\theta \, \mathrm{d}s$, and the divergence theorem is applied to the last term in Eq. (17), the result is

$$\int_A \left\{ \tilde{\phi}^k [\rho_t^s - \dot{\mathbf{x}}_s \cdot \nabla_s \rho^s] + \tilde{\phi}^k \rho^s v_{(\mathbf{n})} (\nabla_s \cdot \mathbf{n}) - \nabla_s \tilde{\phi}^k \cdot \rho^s \mathbf{v}^s + \frac{1}{Pe_s} (\nabla_s \tilde{\phi}^k \cdot \nabla_s \rho^s) \right\} r_s \, \mathrm{d}s + \left\{ \left[\tilde{\phi}^k \rho^s (\mathbf{v}^s \cdot \mathbf{t}) - \frac{1}{Pe_s} \tilde{\phi}^k (\nabla_s \rho^s \cdot \mathbf{t}) \right] r_s \right\} \Big|_{s=0}^{s=s_F} = 0 \tag{18}$$

where the last term in Eq. (18) represents the convective and the diffusive transport of surfactant through both ends of the interfacial domain; this ends are indicated by $s = 0$ and s_F in the arc length coordinate and are located at $z = 0$ and π/α, respectively. Expression (18) easily allows the introduction of the periodic (or symmetric) boundary condition at both extremes of the interface by simply eliminating the last term, i.e. the null transport of solute is imposed in a weak form. It must be noticed that at those points $\partial h/\partial z = 0$, implying that $\mathbf{v}^s \cdot \mathbf{t} = w = 0$ and $\nabla_s \rho^s = \mathrm{d}\rho^s / \mathrm{d}s \mathbf{t} = 0$.

Finally, the term $\nabla_s \cdot \mathbf{n} = -2H = -(\kappa_1 + \kappa_2)$, where κ_1 is the axial curvature and κ_2 is the azimuthal one. Therefore, Eq. (18) can be rewritten in the more computational convenient form

$$\int_A \left\{ \tilde{\phi}^k \left[\rho_t^s - \dot{\mathbf{x}}_s \cdot \frac{\mathrm{d}\rho^s}{\mathrm{d}s} \mathbf{t} \right] - \tilde{\phi}^k \rho^s v_{(\mathbf{n})} (\kappa_1 + \kappa_2) - \left(\frac{\mathrm{d}\tilde{\phi}^k}{\mathrm{d}s} \mathbf{t} \cdot \rho^s \mathbf{v}^s \right) + \frac{1}{Pe_s} \left(\frac{\mathrm{d}\tilde{\phi}^k}{\mathrm{d}s} \mathbf{t} \cdot \frac{\mathrm{d}\rho^s}{\mathrm{d}s} \mathbf{t} \right) \right\} r_s \, \mathrm{d}s = 0 \tag{19}$$

where the curvatures are calculated by

$$\kappa_1 = \frac{\mathrm{d}\mathbf{t}}{\mathrm{d}s} \cdot \mathbf{n}, \qquad \kappa_2 = -\frac{(\mathbf{n} \cdot \mathbf{e}_r)}{r_s} \tag{20}$$

The expressions for the normal and the tangent unit vectors to the free surface (**n** and **t**, respectively) are readily obtained through the isoparametric mapping of coordinates since the free surface is represented by a line where one of the local coordinates presents a constant value (Kistler and Scriven, 1983).

In order to complete just the fundamentals of the numerical technique employed, we must point out the following:

- The spatial tessellation implemented by the Galerkin-finite element technique yields a set of ordinary differential equations in the discrete variables $\mathbf{v}^j(t)$, $p^i(t)$, $\mathbf{x}^j(h^k(t))$ and $\rho^{s^m}(t)$, whose integration in time was carried out with a second order predictor–corrector scheme; for that purpose we chose the Adams–Bashforth formula and the trapezoidal rule as predictor and corrector, respectively.
- The time step was adjusted using a heuristic method proposed by Crisfield (1981) which intends to converge in a constant number of iterations; for that purpose the size of the step is increased or decreased taking in account if convergence in the previous step was attained in a smaller or a larger number of iterations than the target sought. For the present problem this simple procedure proved to be more efficient than various more complicated schemes (cf. Corvalán and Saita, 1991).
- The nonlinear system of algebraic equations and boundary conditions that result at each time step was solved by Newton iteration; typically the targeted number of iterations was two and the process was considered converged when the norm of the difference between two consecutive vector approximations was 10^{-6}, or smaller.

3. Validation of the model

In this section we compare predictions of our model with analytical results produced by Goren (1962), who performed linear stability analysis on the governing equations of the problem, and with experimental results obtained by Goldsmith and Mason (1963).

3.1. Linear stability analysis

Goren (1962) considered the instability of a thin liquid annulus of a given thickness subject to infinitesimal axially symmetric perturbations; for that purpose he solved the Navier–Stokes and continuity equations with appropriate boundary conditions when a small disturbance was introduced. For the limit cases of $Re = 0$ and $Re \to \infty$ he arrived at an analytical expression from which he was able to determine the grow factor of any given disturbance. Finally, for each value of relative initial film thickness (F), the perturbation that grows more rapidly than any other disturbance (i.e. the perturbation whose wave-number is denoted by α^*) was determined by parabolic interpolation about the maximum in the plot of growth factor versus wave-number.

The most dangerous perturbation was also determined using our numerical model. For that purpose we perturbed a stationary annular film of a given thickness by sinusoidal waves of small amplitudes ($\varepsilon_0 < 10^{-3}$) and several values of the wave-number, which are chosen conveniently close to the value determined by Goren. Following the time evolution of the free surface for each disturbance, the corresponding exponential growth rate is easily determined from the slope of the curve: $\ln(h_0)$ versus time, where h_0 is the film thickness at the wave crest ($h_0 = h(0,t)$). Again, a suitable interpolation about the maximum in the curve of growth rate versus wave-number gives our prediction for α^*. Since we are perturbing the free surface location only, the exponential grow is not attained immediately but after a few time steps, when the remaining variables (velocities and pressures) accommodate themselves to the imposed disturbance.

In Table 1 we compare, for several values of relative film thickness (F), the fastest growing wave-number determined with our model and the corresponding one predicted by the linear stability theory (Goren). It is clear the excellent agreement found in all cases assuring the ability of our model to reproduce the earlier steps of the instability, i.e. when the nonlinear characteristics of the system have not become evident yet. The results summarized in Table 1 are also depicted in Fig. 2 where the continuous lines give the fastest growing wave-number predicted by linear stability theory.

Table 1
Fastest growing wave-number predicted (α^*) and concomitant errors

F	$Re = 0$			$Re \to \infty$		
	Goren	Numer.	%error	Goren	Numer.	%error
0.01	0.7141	0.7094	0.66	0.7141	0.7054	1.21
0.1	0.7766	0.7719	0.60	0.777	0.7692	1.00
0.3	0.9576	0.9560	0.17	0.9828	0.9814	0.14
0.5	1.204	1.2018	0.18	1.3480	1.3552	0.53
0.7	1.4487	1.4481	0.04	1.9536	1.9869	1.70
0.9	1.61	1.6382	1.75	4.8500	4.8137	0.75

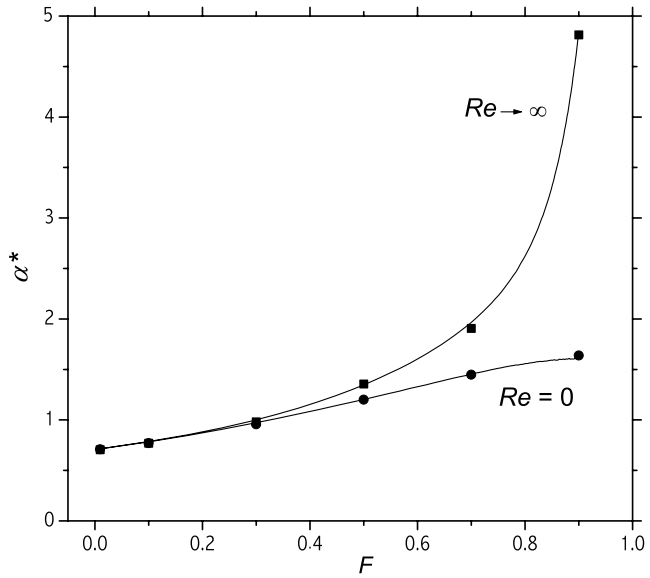

Fig. 2. Fastest growing wave-numbers predicted by linear stability analysis (continuous line) and by this work.

3.2. Nonlinear results

The next step is to compare experimental results with predictions of our model when the evolution of the liquid film is strongly affected by nonlinear effects. Goldsmith and Mason (1963) followed the evolution of the instability of a liquid film in a capillary, by measuring the radial location of the crest of the growing interfacial wave. The radius of the capillary tube employed was 10^{-3} m and the physical properties of the liquid film (glycerol) were 1.25 Pa s, and 1250 kg/m^3 for viscosity and density, respectively; also, the phase surrounded by the annular film originates an interfacial tension of 0.0115 N/m. Since the core phase (ethylene chloride) was a liquid approximately 2500 times less viscous than the annular liquid film, but of a rather similar density, the behavior of the system should well fit the assumptions made in setting up our model, i.e. negligible gravitational effects and a nonviscous core phase.

Goldsmith and Mason determined the initial thickness of the annular film and traced the successive interfacial locations with the aid of photomicrographs; the readings were corrected for refraction error. The quality of the measurements provided by this technique was previously assessed by the authors (cf. Table 2 of G&M) who established, for a dozen cases, a maximum error of approximately 10% and an average error of about 5.2%. Goldsmith and Mason presented two sets of results that, according to their measurements, pertain to relative initial film thickness (F) of 0.19 and 0.26, respectively; they are summarized in Fig. 3 where the radial location of the top of the increasing wave versus time is portrayed. The predictions of our model for the two values of F already mentioned, and also for the error bounds in F of $\pm 5\%$, are depicted in the same figure. When the bubble break-up times are drawn coincidently, the good agreement is evident since the experimental values are clearly located between the predicted bounds.

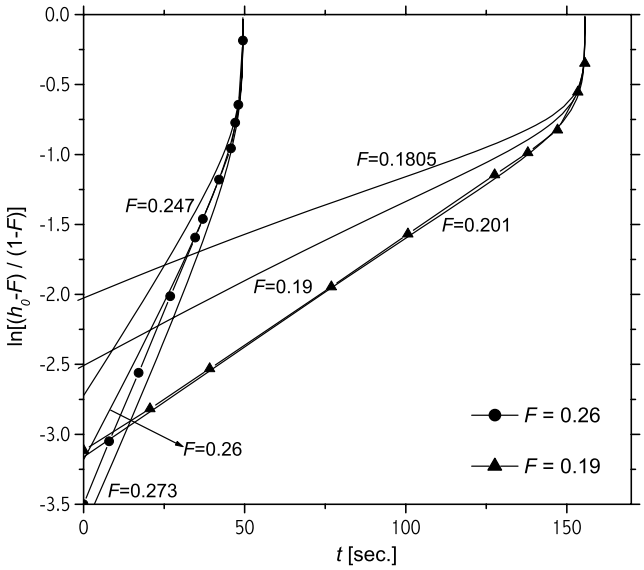

Fig. 3. Radial location of the interfacial wave crest as function of time. Triangles and circles are the experimental results of Goldsmith and Mason for $F = 0.19$ and 0.26, respectively. The continuous lines are the results of the present work for similar values of initial relative film thickness and also for the bounds of ±5% in F.

Although the comparisons just performed are not enough to validate our model beyond any doubt, the agreement observed is rather significant, and we might have reasonable confidence in its predictions. Therefore, in the next section we will use our model as a standard to evaluate simpler ones based on the one-dimensional perturbation flow approximation. We will also show results establishing airway closure times in capillaries and sample results portraying changes in velocity fields—and in airway closure times as a consequence—when surface active agents are present.

4. Computed predictions

4.1. 1-D versus 2-D flow models

In this section we are going to compare predictions obtained from numerical models based on 1-D flow assumptions with those given by our 2-D axisymmetric flow model. In particular, we will compare the predicted times for the Rayleigh instability to be completed; i.e. the so-called airway closure time. Comparisons will be made first considering pure liquids and then, liquids contaminated with insoluble surfactants.

4.1.1. Pure liquids

Gauglitz and Radke (G&R) in 1988 presented a simplified model that represents the motion of thin liquid films in cylindrical capillaries. They arrived at a single evolution equation for a film location following a procedure already employed by Hammond (1983) by which the liquid flow

was approximated as one-dimensional. The model of Hammond was based on a thin film expansion where only the leading terms were retained; thus, the essence of the cylindrical geometry was lost and, though the formation of stable collars was predicted the model was unable to reproduce the bubble break up and the formation of lenses. This drawback was overcome by G&R who retained the circumferential curvature by employing what they called, the small-slope approximation.

Fig. 4 presents for three different values of relative initial film thickness (F), the evolution of the radial location of the wave crest as a function of the dimensionless time. It must be noticed that the initial perturbation imposed was not a small one but it was 50% of the initial film thickness $(h_0/F)_{t=0} = 1.5$. Thus, the perturbation is rather large and the growth rate of the disturbance predicted by both models differs from the start.

The results presented by G&R do not reach the point where the airway closure occurs; nonetheless, the growth rate of the instability at the last time computed is so large that the airway closure occurs almost immediately; consequently, that time can be taken as the predicted closure time. The differences between the predictions of both models are evident, the simpler model overestimates the closure times when the amount of liquid in the film is barely enough to produce the bubble break up ($F = 0.14$); however, as the initial film increases the trend is reversed and for $F = 0.20$ the closure time given by G&R is 30% shorter than our result.

The results of two other one-dimensional flow models have been tested. One of them was presented by Johnson et al. (1991) who employed an ad hoc approximation to include the effect of inertia and the other was published by Halpern and Grotberg (1992) who, as we mentioned before, did not consider inertia forces but introduced a new element; vg. the flexibility of the capillary walls.

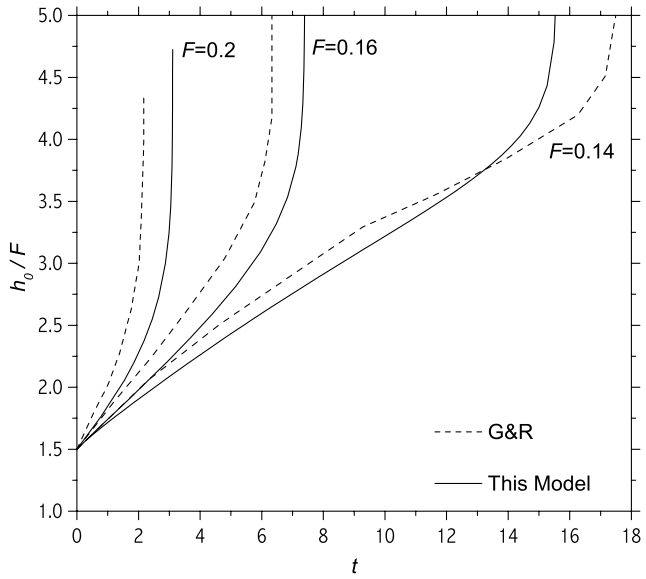

Fig. 4. Predictions of Gauglitz and Radke's model and present model of the radial location of the wave crest versus dimensionless time for three values of F.

Among the cases studied by Johnson we choose one whose dimensionless parameters in our formulation are the following: $Re = 40$, $F = 0.2$, $\alpha = 1.047$ and $\varepsilon_0 = 10^{-3}$; for that system the dimensional closure time given by Johnson et al. was 0.065 s while our model predicted 0.084 s, signifying that the simpler model underestimates the bubble break-up time by approximately 22%.

Halpern and Grotberg (1992) analyzed the Rayleigh instability in flexible capillary tubes; however, they also presented results for a liquid film lining a rigid tube. This case was exactly the one just shown for Johnson's model, except for the inertial forces which were not considered by the authors. Thus, in our formulation the dimensionless parameters representing this system take on the following values: $Re = 0$, $F = 0.2$, $\alpha = 1.047$ and $\varepsilon_0 = 10^{-3}$, and the numerical solution shows that the time needed for the formation of a liquid lens is 77 ms. Again, according to Halpern and Grotberg who stated that the evolution was completed in 60 ms, the 1-D model underestimates the closure time by almost 20%; however, if the dimensionless time values are compared we observe an approximate error of 32%. The reason for this discrepancy is the lack of agreement between the dimensional and dimensionless values given by H&G.

We have also contrasted predictions of successive shapes adopted by the free surface during the instability process; those results are not shown here but, in general, a reasonable good agreement is found between the predictions of the approximated models and our results. Thus, the weakest point of the approximated models seems to be the prediction of the amount of time needed for airway closure completion—a fundamental datum for those performing lung functioning analysis.

4.1.2. Insoluble surfactant

Halpern and Grotberg (1993) introduced the equations accounting for the presence of an insoluble surfactant into their previously developed model for studying the influence of wall flexibility on the airway closure time (H&G, 1992). In this version of the model, they balanced the viscous shear stresses with the surface tension gradients induced by surface convection under the presence of surfactants; in addition, they introduced an interfacial mass balance equation for the solute adsorbed at the interface and an equation of state that linearly relates the surface tension to the local concentration of adsorbed surfactant. Again, most of the results presented in that work were for capillary tubes of flexible walls; nonetheless, three of them considered rigid tubes and the values of the elasticity number examined were 0.0, 0.4 and 8.0, respectively. The system analyzed by Halpern and Grotberg can be represented in our model by the following values: $Re = 0$, $F = 0.2$, $\alpha = 1.047$ and $\varepsilon_0 = 10^{-3}$ and, since they neglected the transport of solute by interfacial diffusion: $Pe_s \to \infty$ ($Pe_s = 10^6$).

In Table 2 the dimensionless closure times presented by H&G for the three values of the elasticity number are compared with predictions of our model. When the elasticity number (β) is zero, i.e. the adsorbed solute is an inert agent, the results shown are those already presented in the previous section in which the simpler model underestimates the closure time by 32.1%. The error becomes larger when the elastic action induced by interfacial concentration gradients are considered; thus the underestimation reaches 58.1% for $\beta = 0.4$ and amounts almost 40% for $\beta = 8.0$. In addition to the different closure times predicted, it is interesting to observe the different sensitivity to the elasticity number presented by these two models. While predictions of the simpler model change rather slowly when β is varied between 0 and 8, the more accurate model show that closure times rapidly change when β is 0.4 or smaller, and only marginal variations occur when β is increased beyond this value. It should be remarked that the interfacial mass balance equations

Table 2
Effect of β on dimensionless closure times

β	t_C (H&G)	t_C (2-D model)	%error
0.0	33.7	49.62	32.1
0.4	88.05	210.25	58.1
8.0	129.25	214.05	39.6

employed in both models, as well as the constitutive equation relating the surface tension to the local concentration of adsorbed surfactants, are in this case completely equivalent. Therefore, the differences just observed should be originated in the already existing differences in the flow field which become enhanced when the adsorbed active solute interacts with the velocity field.

Otis et al. (1993) also studied the role of surfactant in airway closure. These authors were mainly interested on the effects of surfactants on lung conduits; thus, in most of their analysis they considered a capillary that changes its volume in order to mimic the contracting process suffered by a respiratory bronchiole during expiration. The model employed by Otis et al. was built on the one developed by Johnson et al. (1991) by adding the appropriate equations to include both the capillary size variation and the presence of an insoluble surfactant. Nonetheless, they also examined the case of a noncontracting tube and in Fig. 5 we compare their predictions with our results.

The values of the parameters used to obtain the results depicted in Fig. 5 are typical of a terminal or respiratory bronchiole, those values were summarized by Otis et al. (1993) in their Fig. 8 and when they are used to evaluate the dimensionless parameters used in this work the result is $Re = 40$, $F = 0.2$, $\alpha = 1.047$ and $\varepsilon_0 = 10^{-3}$ and $Pe_s = 4032$; this last value comes from the adoption of D_s (the interfacial diffusion coefficient) equal to 10^{-8} m^2/s.

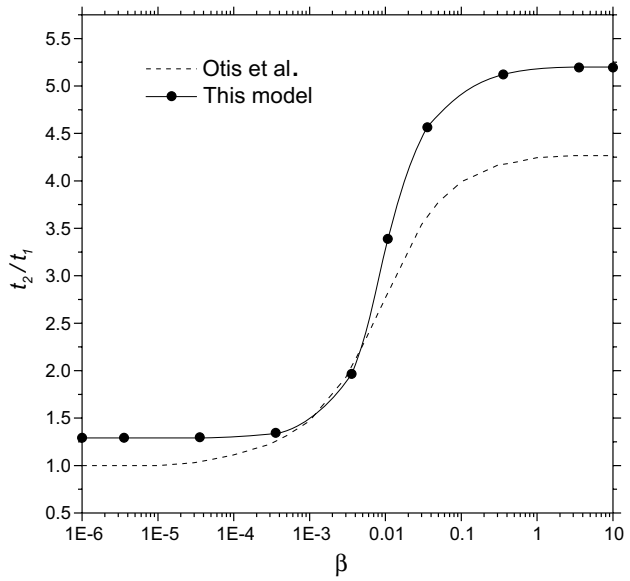

Fig. 5. Comparison of relative airway closure time versus elasticity number obtained with the present model and those given by Otis et al. The result of Otis et al. for a clean interface ($\beta = 0$) is used as the reference closure time (t_1).

Fig. 5 portraits the closure time predicted for values of the elasticity number (β) varying between 10^{-6} and 10. The closure times are measured relative to the closure time obtained by Otis et al. for a clean interface; therefore, the value of the relative closure time given by these authors approaches one when $\beta \to 0$. The differences observed between the predictions of the two models are rather similar to those just reported when we made comparisons with H&G's results; again, the simpler model underestimates the airway closure time by an amount that is small when β is in the range 10^{-2}–10^{-3} and reaches 22% when the interface is clean. Though in this case the simpler model shows better agreement with our results, once more its closure time predictions clearly present less sensitivity to the changes in the elastic effects than the 2-D model.

4.2. Axisymmetric model: numerical results

In the first part of this section we present our predicted dimensionless time for the Rayleigh instability to be completed (closure time) when pure liquids films of various initial thickness are lining the inner walls of capillaries. We believe that this comprehensive information that allows to obtain the actual closure times when the geometric and physical parameters of a given system are introduced, has not been published before. Also, we exemplify the influence of surfactants on the delay of the instability for a particular initial thickness and several values of the elasticity number.

In the second part we illustrate the information that might be drawn from a 2-D model; to this purpose we observe the changes produced in the flow fields as the Rayleigh instability starts and proceeds toward its completion.

4.2.1. Closure times

The results depicted in Fig. 6 are the dimensionless closure times predicted by our model. The maximum value of the Reynolds number considered in Fig. 6 was set assuming a maximum

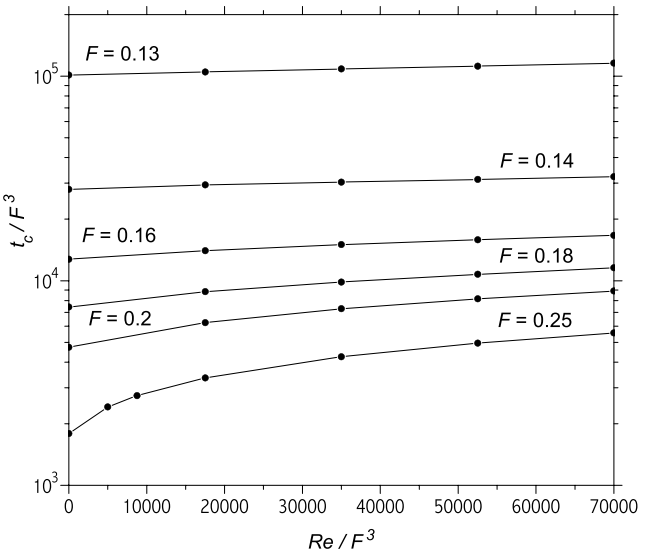

Fig. 6. Present model predictions of dimensionless closure time versus Reynolds number for several values of initial film thickness.

capillary radius of 1 mm and the physical properties of water; thus, $Re_{\max} = 7 \times 10^4 \times F^3$. The results portrayed were obtained using the most unstable wave-numbers predicted by linear stability analysis in the following way: since $\alpha^* = f(F, Re)$, for all points lying on the extreme right in Fig. 6 we employed the wave-number predicted by Goren when $\alpha^* = f(F, Re \to \infty)$, while for the points lying on the extreme left we employed the Goren's results for $\alpha^* = f(F, Re = 0)$. Then, for the points at intermediate Reynolds we just used a linear interpolation since these two extreme values differ at most by 2.83% when $F = 0.25$, while for the remaining cases portrayed in Fig. 6 that difference is less than 1.2%.

When the initial film thickness is smaller than 0.18 Fig. 6 shows that closure times rapidly increase as the initial film becomes thinner; also, the small slope of the curves indicates that they are a weak function of the Reynolds number. Then, the dimensional closure times should depend almost linearly on liquid viscosity.

In order to exemplify the effect of the elasticity number on closure times we have arbitrarily selected the system represented by the curve of $F = 0.18$ in Fig. 6. In Fig. 7 we observe how this curve is displaced toward larger values of closure times as the elasticity number is increased. It is also clear that closure times are more sensitive to the action of surfactants when the elasticity number varies between 10^{-3} and 0.1, this feature was already observed in the results shown in Fig. 5. It must be remarked that the results portrayed in Fig. 7 are practically insensitive to diffusive effects since the interfacial Péclet number presents rather large values considering that D_s is in the range of 10^{-8}–10^{-9} m^2/s.

4.2.2. Surfactant effects on flow fields

In previous sections we have seen the action of surfactants on the time needed for the Rayleigh instability process to be completed; here, our goal is to visualize how their action change the

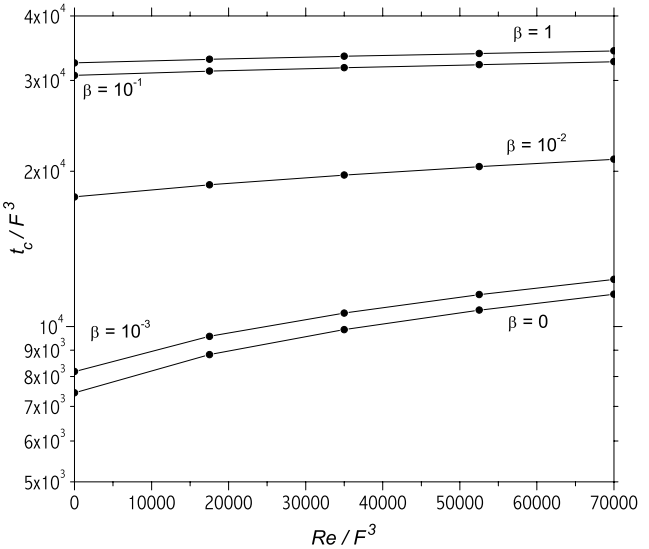

Fig. 7. Present model predictions of dimensionless closure time versus Reynolds number for $F = 0.18$ and several values of the elasticity number.

interfacial dynamics of the unstable films giving rise to forces that oppose the capillary driven instability. For that purpose we choose the system whose closure times were portrayed in Fig. 5 for different values of β, and we will observe the temporal evolution of the instability for two values of β: 3.6×10^{-3} and 0.36, respectively.

Figs. 8 and 9 summarize through five instants, the temporal evolution of the instability when the adsorbed solute is a weak surface active agent ($\beta = 3.6 \times 10^{-3}$). The first result of the sequence shows the streamlines and the values of the interfacial variables just after the beginning of the instability, while the last represents the state of the system near the end of the process; they are

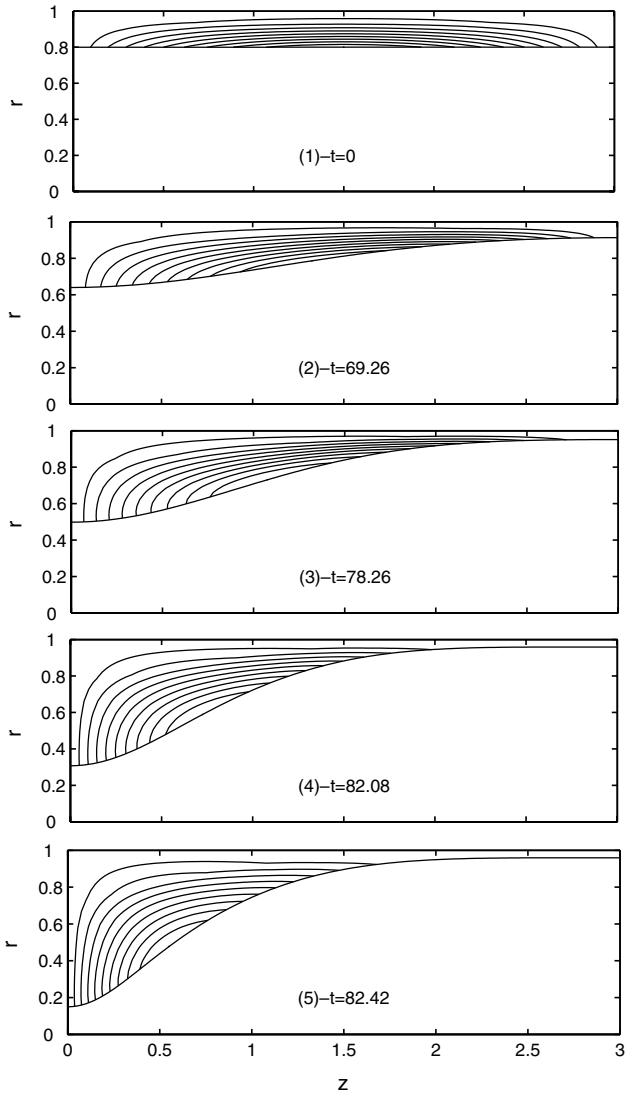

Fig. 8. Streamlines showing the Rayleigh instability flow at five instants (1–5) when a weak surface active agent ($\beta = 3.6 \times 10^{-3}$) is present.

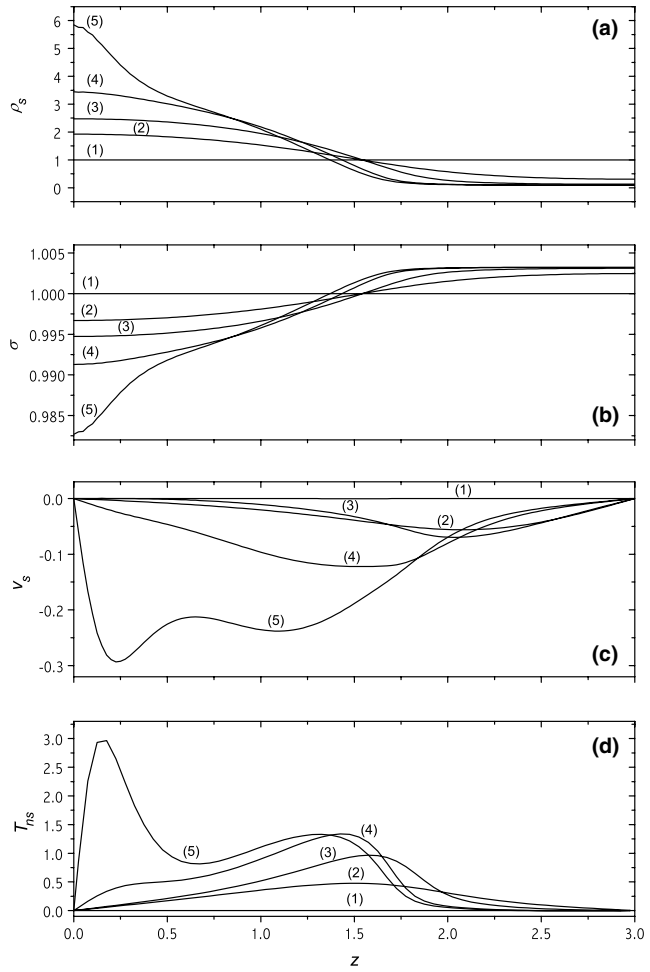

Fig. 9. Interfacial properties corresponding to the five instants portrayed in Fig. 8; (a) interfacial concentration of surfactant, (b) surface tension, (c) tangential interface velocity, and (d) interfacial tangential stresses.

characterized with (1) and (5), respectively. Intermediate steps are marked (2) to (4) for increasing times.

Fig. 8 portraits the instantaneous streamlines at the five instants just mentioned; it does not show any relevant feature except for the varying speed of the process, which is very slow at the beginning of the instability, and very fast near the end when the liquid collar neck becomes small and the transverse free surface curvature at that point increases without limits. More significant are the plots of the interfacial variables shown in Fig. 9; there, the concentration of solute, the surface tension, the fluid surface velocity and the tangential stress at the interface are shown along the axial coordinate for the five instants defined in Fig. 8.

Fig. 9(a) shows the surface concentration of surfactant which is practically uniform at step (1); but, as the instability develops, the right part of the domain becomes depleted of solute while the

opposite occurs on the left part. This variation is partially due to the interfacial convective transport of solute since the velocity at the interface is always negative as it is indicated in Fig. 9(c) (the positive arc length along the surface is defined from left to right); however, near the left end of the domain the most important contribution is produced by the interface itself, which shrinks with the evolution of the instability leaving less interfacial area available for the solute that was already there.

Since the interfacial concentration of surfactant decreases as we move toward larger arc-length values, the opposite happens with the surface tension as Fig. 9(b) illustrates. Thus, along the surface, a positive surface tension gradient results and, consequently, a positive interfacial tangential stress arises (Fig. 9(d)). This interfacial stress opposes the tangential component of the surface velocity, but is not strong enough as to change its direction because we are considering a rather weak surfactant; nonetheless, the evolution of the instability is retarded and is completed in a lapse of time twice as long as the one needed for a clean interface (cf. Fig. 5).

The results presented in Fig. 8 seem to evidence that no significant changes exist in the flow fields when the interface is contaminated with a weak surfactant; actually, the streamlines shown are quite similar to the streamlines observed when the interface is clean and the main difference between these two cases is the time needed to reach each configuration. Nonetheless, the differences exist, and they are revealed by the interfacial variables and the values they adopt as the instability advances.

We are now going to examine a case for an adsorbed solute whose surface activity is stronger ($\beta = 0.36$). The results obtained in this case are ordered as in the previous one; i.e. Figs. 10 and 11 are the exact counterpart of Figs. 8 and 9, respectively. In addition, we have chosen the instants shown in Fig. 10 in such a way that they present similar progresses in the instability process to those shown in Fig. 8.

When Figs. 8 and 10 are compared, it becomes clear that the successive shapes adopted by the interface during the advance on the instability do not depend upon the strength of the surfactant adsorbed. Actually, according to our numerical computations, the interfacial area does not depend on the presence of any insoluble surfactant and is kept practically constant during the whole process. In fact, for the instants shown in both figures, our results indicate that the interfacial area is never reduced by more than 1.25% from its initial value of 15.082. Thus, the main action of the surfactant seems to be the delay produced in the evolution of the instability, and this is accomplished by modifying the interfacial stresses which, in turn, produce changes in the flow field.

The instantaneous streamlines shown in Fig. 10 look alike to those shown in Fig. 8, except for the region where they contact the free surface indicating that the tangential velocity at the interface is now positive. Also, it is evident that this motion induces a swirl which is located close to the free surface; this swirl strengthens and moves toward the left of the domain as the collar grows.

The interfacial variables and their change with time are exhibited in Fig. 11. If we compare the curves of interfacial distribution of solute as well as the surface tension along the interface for both values of the elasticity number (3.6×10^{-3} and 0.36), we may observe that they are rather similar (Figs. 9(a,b) and 11(a,b)). However the scales are completely different and the maximum interfacial concentration of solute in this case is about 1.16 when in the previous case was almost 6.

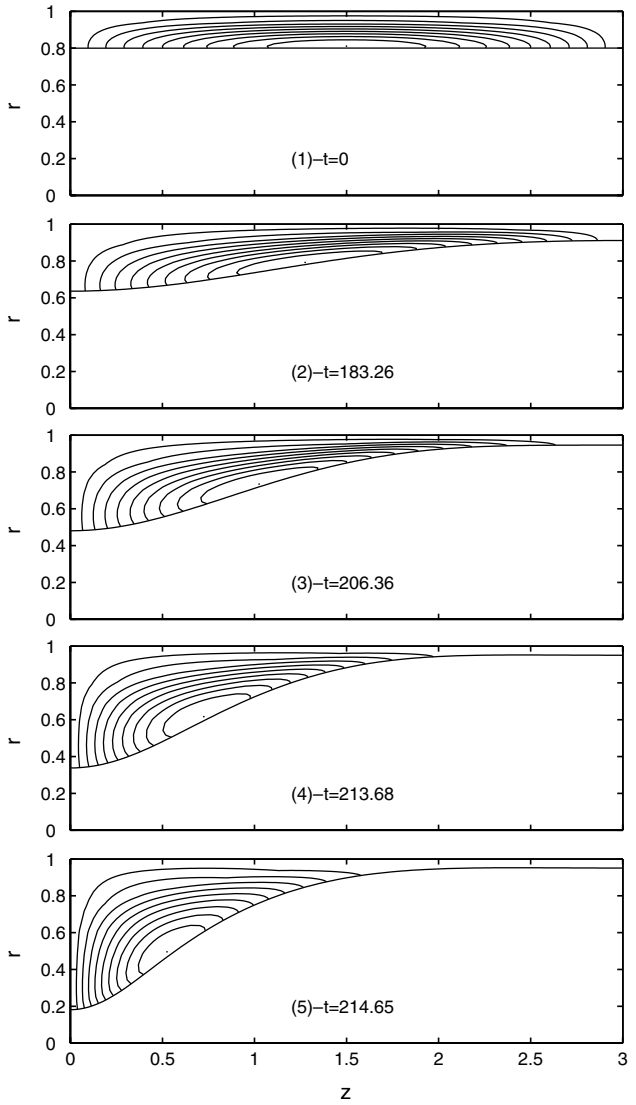

Fig. 10. Streamlines showing the Rayleigh instability flow at five instants (1–5) when a stronger surface active agent ($\beta = 0.36$) is present.

Despite the smaller changes in surface concentration, the relative variation of surface tension at $z = 0$ is larger due to a larger elasticity number (5.85% versus 1.7% in Fig. 9(a)). A similar effect is produced on the tangential stresses at the interface, which now are large enough to totally reverse the interfacial fluid motion, inducing the swirl depicted in Fig. 10. Thus, the net flow rate toward the collar is reduced and the evolution speed of the instability diminishes too; consequently, the airway closure occurs at $t = 214.63$ which is 2.6 times larger than the case portrayed in Figs. 8 and 9.

When the system reaches the final steps of the instability, i.e. when the radius of the airways passage has been reduced to 40% or less of the capillary radius, the liquid lobe acquires its

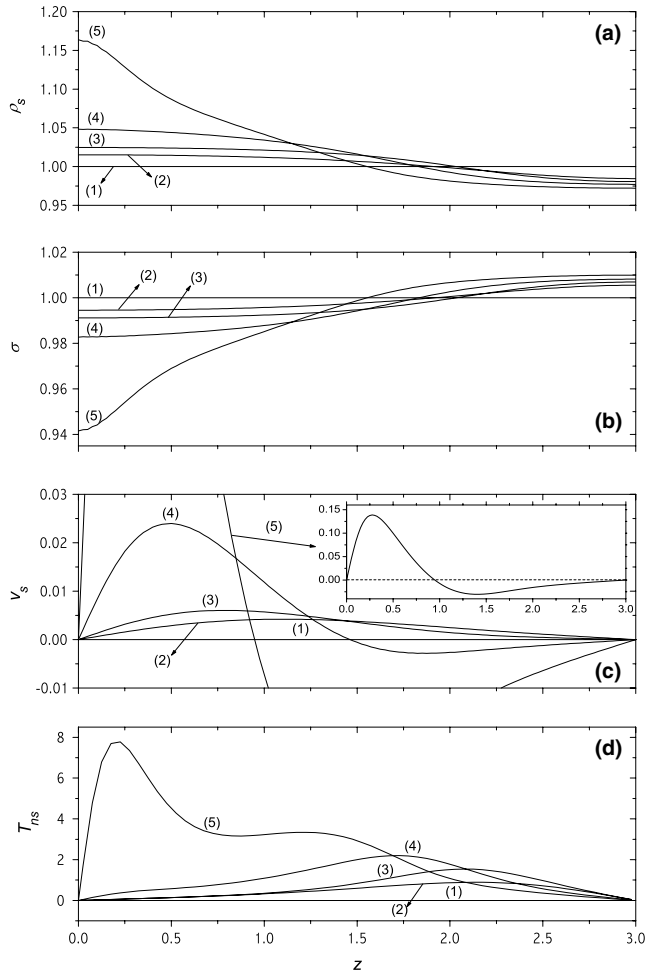

Fig. 11. Interfacial properties corresponding to the five instants portrayed in Fig. 10; (a) interfacial concentration of surfactant, (b) surface tension, (c) tangential interface velocity, and (d) interfacial tangential stresses.

maximum growing speed; but, at the same time the retarding action induced by the adsorbed solute is maximum too. Fig. 11 shows the interfacial variables attaining their largest values at instant (5); in particular, the magnitude of the peak presented by the interfacial velocity indicates the existence of a strong interfacial convective effect that is working to smooth out the free surface. On the other hand, the tangential component of the interfacial velocity on the right of the domain reverses its direction; this feature indicates that the local convective effects have become large enough there to overcome the action of the surfactant.

The results shown in this section, in particular those presented in Figs. 10 and 11, are helpful to understand the complex events generated by an insoluble surfactant acting on an interface, and how these effects are conveyed to the bulk phase by viscous effects. In fact, they show that Rayleigh instability is delayed by the combined action of a tangential interfacial motion and a secondary flow motion in the bulk; both movements together oppose the main flow driven by

capillary pressure. Obviously, the delaying effect of the flow swirl can not be accounted for by the simpler models based on the one-dimensional flow assumption; and this explain why their relative errors in airway closure time become larger when surface active agents are present.

5. Concluding remarks

In this work we analyzed the Rayleigh instability of a thin film lining the inner walls of a capillary tube; to this end we put forward a two-dimensional model that was numerically solved using a suitable technique based on the Galerkin-finite element method.

The new model was validated not only at the former steps of the instability, i.e. when the system presents an almost linear behavior, but also when the evolution of the film was strongly affected by nonlinear effects. In the first case the predictions were compared with the results of the linear stability analysis performed by Goren and, in the second case, they were compared with experiments carried out by Goldsmith and Mason. In both instances we found excellent agreement.

The present formulation was subsequently used to evaluate simpler one-dimensional representations previously employed in the analysis of Rayleigh instability. The comparisons were made for both, pure a contaminated liquid films; it was found that the simpler models represent the instability process with reasonable accuracy, except for the speed of the evolution. In fact, they predicted shorter times for the completion of the instability process and those underestimations were more pronounced when the liquid film was contaminated with surface active agents.

The times needed to produce the airway closure are crucial in studying certain biological process (e.g. lung functioning analysis); therefore, to be used as a guide, we computed closure times in rigid capillaries for different values of the geometric and physical parameters. At present, these results would be the most accurate predictions available for rigid conduits, as it is suggested by the excellent agreement obtained when our representation was validated with experiments.

Finally, we showed the successive changes taking place in the flow fields when the Rayleigh instability occurs under the presence of surfactants. These results not only exemplify the wealth of information that might be extracted from the predictions, but also explain why the differences between the closure times predicted by 1-D and 2-D formulations become larger when surfactants are present.

When the thickness of pure liquid films are about one order of magnitude smaller than the capillary radius, an accurate representation of the system might not be justified if a simpler one can provide almost similar results with less computational cost. However, if the film thickness is of the order of the capillary radius, as it usually happens when the film is lining the external walls of a capillary (or a filament), or if the liquid film is contaminated with surfactants, a more realistic two-dimensional model must be used to obtain reliable predictions.

Acknowledgements

This work has been supported by funds granted by the Universidad Nacional del Litoral, CONICET and ANPCyT.

References

Corvalán, C.M., Saita, F.A., 1991. Automatic step-size control in continuation procedures. Comput. Chem. Eng. 15, 729–739.

Crisfield, M.A., 1981. A fast incremental iterative solution procedure that handles 'snap-through'. Comput. Struct. 13, 55–62.

Edwards, D.A., Brenner, H., Wasan, D., 1991. Interfacial transport processes and rheology. In: Brenner, H. (Ed.), Butterworth–Heinemann Series in Chemical Engineering. Butterworth–Heinemann.

Gauglitz, P.A., Radke, C.J., 1988. An extended evolution equation for liquid film breakup in cylindrical capillaries. Chem. Eng. Sci. 43, 1457–1465.

Giavedoni, M.D., 1995. A numerical study of the two-dimensional dynamic behavior of a thin liquid film subject to a vertical oscillation. Ind. Eng. Chem. Res. 34, 356–365.

Giavedoni, M.D., Saita, F.A., 1997. The axisymmetric and plane cases of a gas phase steadily displacing a Newtonian liquid—A simultaneous solution of the governing equations. Phys. Fluids 9, 2420–2428.

Giavedoni, M.D., Saita, F.A., 1999. The rear meniscus of a long bubble steadily displacing a Newtonian liquid in a capillary tube. Phys. Fluids 11, 786–794.

Goldsmith, H.L., Mason, S.G., 1963. The flow of suspensions through tubes. II-Single large tubes. J. Colloid Sci. 18, 237–261.

Goren, S., 1962. The instability of an annular thread of fluid. J. Fluid Mech. 12, 309–319.

Halpern, D., Grotberg, J.B., 1992. Fluid-elastic instabilities of liquid-lined flexible tubes. J. Fluid Mech. 244, 615–632.

Halpern, D., Grotberg, J.B., 1993. Surfactant effects on fluid-elastic instabilities of liquid-lined flexible tubes: a model airway closure. J. Biomech. Eng. 115, 271–277.

Hammond, P.S., 1983. Nonlinear adjustment of a thin annular film of viscous fluid surrounding a thread of another within a circular cylindrical pipe. J. Fluid Mech. 137, 363–384.

Johnson, M., Kamm, R.D., Ho, L.W., Shapiro, A., Pedley, T.J., 1991. The nonlinear growth of surface-tension driven instabilities of a thin annular film. J. Fluid Mech. 233, 141–156.

Kistler, S.F., Scriven, L.E., 1983. Coating flows. In: Pearson, J.R.A., Richardson, S.M. (Eds.), Computational Analysis of Polymer Processing. Applied Science Publishers, New York.

Kwak, S., Pozrikidis, C., 2001. Effect of surfactants on the instability of a liquid thread or annular layer—Part I: Quiescent fluids. Int. J. Multiphase Flow 27, 1–37.

Otis, D.R., Johnson, M., Pedley, T.J., Kamm, R.D., 1993. Role of pulmonary surfactant in airway closure: a computational study. J. Appl. Physiol. 75, 1323–1333.

Queré, D., 1999. Fluid coating on a fiber. Ann. Rev. Fluid Mech. 31, 347–384.

Severino, M., Giavedoni, M.D., Saita, F.A., 2003a. Soluble surfactant effects on the displacement of a gas/liquid interface between parallel plates. Int. J. Heat Tech. 21, 37–42.

Severino, M., Giavedoni, M.D., Saita, F.A., 2003b. A gas phase displacing a liquid with soluble surfactants out of a small conduit: the planar case. Phys. Fluids 15, 2961–2972.

Tomotika, S., 1935. On the instability of a cylindrical thread of a viscous liquid surrounded by another viscous fluid. Proc. Roy. Soc. A 150, 322–337.

Weber, C., 1931. Zum Zerfall eines Flüssigkeitsstrahles. Z. Angew. Math. Mech. 11, 136–154.

Wong, H., Rumschitzki, D., Maldarelli, C., 1996. On the surfactant mass balance at a deforming fluid interface. Phys. Fluids 8, 3203–3204.